

Chapter 3

Theoretical discussion of quenched narrow-line laser cooling

Now that we understand the need for quenched narrow-line laser cooling (QNLC) for atoms having extremely narrow-linewidth transitions, I would like to explore the theory behind QNLC, focusing on QNLC of ^{40}Ca atoms. In this chapter I investigate two distinct forms of QNLC: a scheme of step-wise excitation and one of simultaneous quenching and cooling. For a step-wise method of excitation with pulses of cooling light followed by quenching, it is difficult to find an analytic solution with which to elucidate the physical manifestation of the cooling. It is possible, however, to gain intuition about the physical nature of this cooling by simulating pulsed QNLC with a Monte Carlo (MC) method. Through MC simulations I will explore many different permutations of the pulsed-cooling method. The theory behind simultaneous cooling, where the cooling and quenching light access the atoms at the same time, is just an extension of Doppler cooling with the added complication that the choice of such a narrow transition for cooling requires quenching of the excited population in order to speed up the cooling process. Cooling on a narrow transition also limits the Doppler coverage of the cooling light, necessitating the use of broadened cooling laser light in order to allow more of the initial velocity distribution to be cooled. I will explore how this method has been used to both cool and trap alkaline-earth atoms in three dimensions to the narrow-line Doppler cooling limit.

3.1 Pulsed QNLC

For QNLC of ^{40}Ca we use the narrow 657 nm (red) $^1S_0(4s^2) \rightarrow ^3P_1(4s4p)$ transition to excite atoms in a velocity selective manner, and use the 552.267 nm (green) $^3P_1(4s4p) \rightarrow ^1S_0(4s5s)$ transition to quench the 3P_1 state. (An energy level diagram is shown in Figure 3.1) In our realization of pulsed QNLC, a pulse of 657 nm light

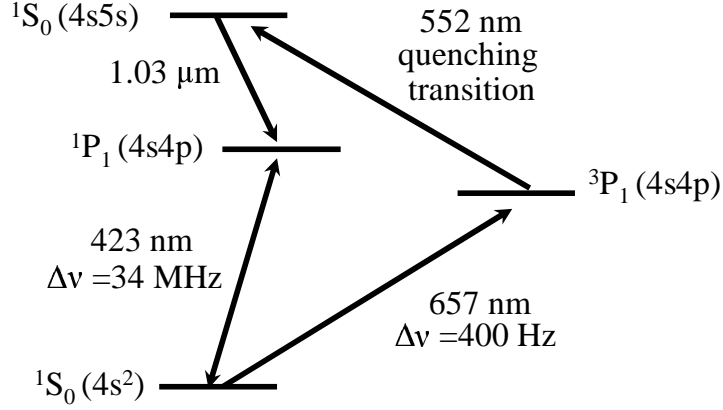


Figure 3.1: Relevant energy levels in ^{40}Ca for quenched narrow-line laser cooling

detuned to the red of resonance excites a velocity class of atoms resonant with the detuned laser light, with a velocity width corresponding to the the inverse pulse length $1/\tau_p$. (This is in frequency units, which translates into the velocity of the atoms by using the simple Doppler-shift relation $-\vec{k} \cdot \vec{v} = 2\pi\nu$, where \vec{k} is the wave vector of the light, \vec{v} is the velocity of the atom, and ν is the frequency shift from resonance.) A pulse of 552 nm quenching light follows this 657 nm pulse, and quickly pumps the atoms to the ground state via the $^1S_0(4s5s) \rightarrow ^1P_1(4s4p)$ transition. Repetitions of this excitation + quenching cycle can significantly cool the atoms through the selective resonance condition that preferentially reduces the velocity of the majority of the excited atoms. Since this cooling processes uses cooling and quenching pulses separated in time, we can consider the three level ($^1S_0(4s^2) \rightarrow ^3P_1(4s4p) \rightarrow ^1S_0(4s5s)$) system as two uncoupled two-level systems, each playing a separate and independent role, making the

pulsed version of QNLC conceptually more straightforward than its simultaneous and cw counterpart.

The strength and utility of pulsed QNLC comes from the velocity selectivity of the narrow-line cooling pulses. But to understand where this selectivity comes from, we must first understand how laser light excites atomic transitions. In the two-level case, this problem was first solved exactly by Rabi in 1937, with respect to magnetic, rather than light field, resonance.[37] For a two level system with atoms interacting with a light field, we can write an atomic wave function $\Psi(t)$ such that

$$\Psi(t) = \sum_k c_k(t) \psi_k(\vec{r}) e^{-i\omega_k t} \quad (3.1)$$

where $c_k(t)$ includes all the time dependent information of the k^{th} state, $\psi(\vec{r})$ gives all the positional information of the k^{th} state, and $\hbar\omega_k$ is the energy of the k^{th} state. For our two-level system, $k = 1$ refers to the atomic ground state and $k = 2$ to the excited state.

We are considering a system with a Hamiltonian

$$H = H_0 + H_{lightfield} \quad (3.2)$$

where H_0 is diagonal in the ψ basis (with eigen energies $\hbar\omega_1$ for the ground state and $\hbar\omega_2$ for the excited state.) $H_{lightfield}$ describes the off-diagonal coupling of the two levels. We know from quantum mechanics that

$$H\Psi = i\hbar \frac{d}{dt} \Psi \quad (3.3)$$

which, when applied to equation 3.1, gives us two coupled equations involving the ground and excited states.

$$i\hbar \frac{d}{dt} c_1(t) = c_2(t) H'_{12}(t) e^{-i\omega_{21}t} \quad (3.4)$$

and

$$i\hbar \frac{d}{dt} c_2(t) = c_1(t) H'_{21}(t) e^{i\omega_{21}t} \quad (3.5)$$

where $H'_{ij}(t)$ is the matrix element $\langle \psi_i | H_{lightfield} | \psi_j \rangle$ and ω_{21} is the frequency difference between the two energy levels ($\omega_2 - \omega_1$).

In the case of laser light interacting with an atomic system, we can write $H_{lightfield}$ as

$$H_{lightfield} = -e\vec{E}(\vec{r}, t) \cdot \vec{r} \quad (3.6)$$

where e is the electron charge, \vec{E} is the electric field operator, and $\frac{\vec{r}}{|\vec{r}|}$ is the direction of the atomic dipole moment. For plane wave radiation travelling in the \hat{z} direction, $\vec{E}(\vec{r}, t)$ can be written as

$$\vec{E}(\vec{r}, t) = E_0(t)\hat{e}\cos(kz - \omega_l t) \quad (3.7)$$

where $E_0(t)$ is the time-dependent amplitude of the electric field, k is the magnitude of the wave vector of the light field, z is the distance along the \hat{z} axis, and ω_l is the laser frequency. We can then rewrite H'_{21} from equation 3.5 as

$$H'_{21} = \hbar\Omega(t)\cos(kz - \omega_l t) \quad (3.8)$$

where $\Omega(t)$, often called the Rabi frequency, is defined as

$$\Omega(t) = -\frac{eE_0(t)}{\hbar}\langle 2|\vec{r}|1\rangle \quad (3.9)$$

where \vec{r} is the electron coordinate in the electric dipole approximation and $\langle 2|\vec{r}|1\rangle$ is its expectation value.

If we assume a square light pulse in time

$$E_0(t) = \begin{cases} E_0 & 0 \leq t \leq T \\ 0 & t < 0, t > T \end{cases}$$

which has a fixed amplitude over time T , $\Omega(t)$ becomes a constant with respect to time, and it is a simple matter to solve the two coupled time dependent equations. For c_2 , which is now no longer time dependent, we arrive at the following solution

$$c_2 = -i\frac{\Omega}{\Omega_{Gen}}\sin\frac{\Omega_{Gen}T}{2}e^{-i\delta T/2} \quad (3.10)$$

where the generalized Rabi frequency, Ω_{Gen} , equals $\sqrt{\Omega^2 + \delta^2}$ and $\delta = \omega_l - \omega_{21}$ is the detuning between the laser frequency and the atomic resonance. To get the probability that an atom is in the excited state after some time, T , one only needs to square $|c_2|$.

$$|c_2|^2 = \frac{\Omega^2}{\Omega_{Gen}^2} \sin^2 \frac{\Omega_{Gen} T}{2} \quad (3.11)$$

You can see from equation 3.11 that the excitation probability will be the greatest when $\Omega_{Gen} T = \pi$. The probability is only equal to 1 when the detuning δ between the laser and the atomic resonance (from the atoms' frame of reference) is zero *and* the pulse length times the Rabi frequency has an area of π , hence the terminology of “ π -pulse” to describe a pulse of light that excites an atom with 100 % probability. In the laboratory frame we must replace δ with Δ , which is the sum of the laser detuning *and* the Doppler shift due to the velocity of the atom, $\omega_D = -\vec{k} \cdot \vec{v}$, where \vec{k} is the wave number of the light and \vec{v} is the atom's velocity in the lab frame. In this way the excitation probability depends of the velocity of the atoms. In essence, because of their non-zero velocity, the atoms see the laser light (in their reference frame) as detuned due to the Doppler shift. The Δ term writes this directly into the excitation probability. In my simulations I have not included the recoil frequency shift ($\nu_{1 \rightarrow 2} = \nu_0 + 11.5$ kHz, $\nu_{2 \rightarrow 1} = \nu_0 - 11.5$ kHz), which is due to energy conservation in the atom-photon system. This change in the frequency is small with respect to the cooling laser detunings and the spectral width of the pulses, and should not affect these simulation results. (However, this small shift may become more significant in the cooling process for the third-stage cooling I describe later in this chapter.)

Figure 3.2 shows a simulation of the thermal Maxwell-Boltzmann velocity distribution of Ca atoms with an initial $v_{rms} = 70$ cm/s (as is typical for Doppler cooling on the 423 nm transition) after the application of one π -pulse of duration $\tau_p = 5$ μ s, which has been detuned $1/\tau_p$ from resonance. Figure 3.2(a) shows the velocity distribution of the atoms remaining in the ground state and Figure 3.2(b) shows the excited state

velocity distribution of atoms that were excited by the π -pulse. One can clearly see the atoms transferred out of the ground state with the sinc^2 excitation spectrum, obvious in its distinctive excitation probability lineshape. Not only does this sinc^2 probabil-

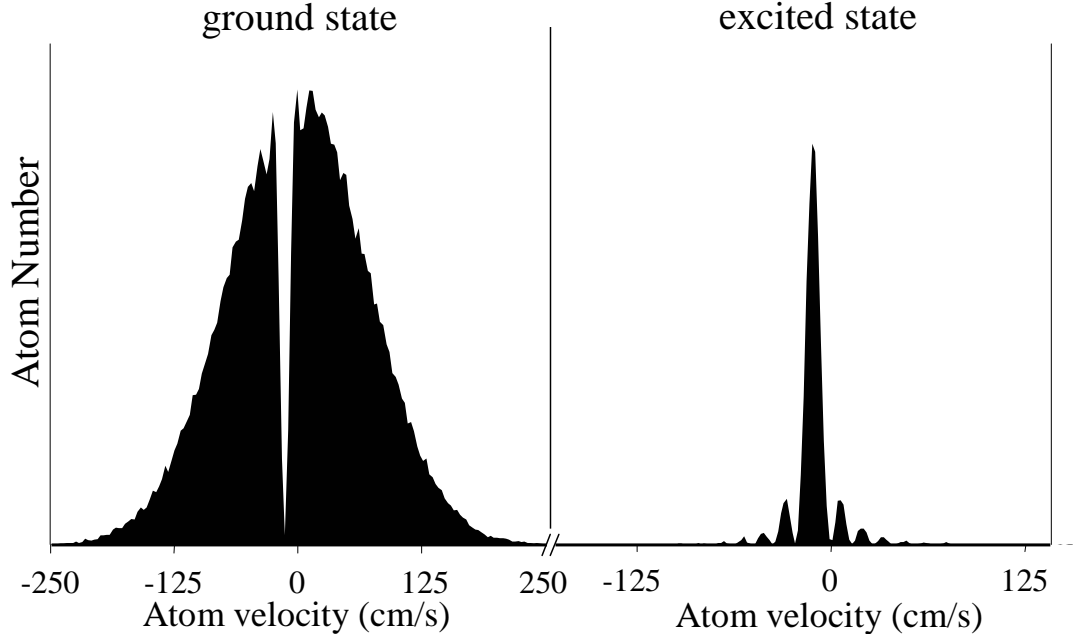


Figure 3.2: Velocity distributions of ground and excited state atoms after an incident 657 nm, 5- μs π -pulse detuned $1/\tau_p$.

ity distribution fall out of the derivation of the excitation probability due to a square cooling pulse (such as the red π -pulses with constant amplitude that we use for our quenched cooling), but one should note that the Fourier transform of a square pulse in time gives a sinc^2 lineshape in the frequency domain.

Key to our cooling scheme is the first zero in the sinc^2 excitation probability. By appropriately detuning the cooling light, atoms can be pushed with the force of the initial cooling and quenching photon recoils and the recoils from spontaneous decay during quenching into these velocity states of near-zero excitation probability where they will most likely not be re-excited. In order to create narrow velocity distributions centered around zero velocity, one might assume that we must simply detune the light

such that the first zero in the sinc^2 probability distribution coincides with zero velocity (as is demonstrated in simulated Figure 3.2). In practice, this is not so straight forward, as I will explain in the next section. By sending the detuned light into the atom trap first from the right and then from the left, atoms are excited in 1-D within some absolute value of velocity and are slowed until they fall into the “hole” near zero velocity and can no longer be excited. These atoms will then remain in this dark state, impervious to excitation by the light fields while we continue to cool the other atoms.

Let us consider a typical cooling pulse sequence in more detail. The sequence commences with a π -pulse of light on the narrow transition. Due to the relatively long lifetime of this transition ($\tau_{Ca} \sim 400\mu\text{s}$), the relevant frequency spectrum of the excitation light is Fourier-transform limited for pulse times $\tau_p < \tau_{Ca}$ and thus can be (in principle) modified to optimize the cooling process. (Note: this is even the case when the Doppler width is $> 1/\tau_p$, where a scan of the velocity distribution will not be Fourier-transform limited; the narrow-line cooling light selects Fourier-transform-limited velocity slices out of the much larger Doppler distribution.) Via the Doppler shift, atoms within a certain velocity range (matching the frequency spectrum of the light pulse) are excited and the absorbed photon imparts one recoil of momentum in the direction of the applied pulse to each excited atom (refer to Figure 3.3.) Thus we are able to exploit the narrow clock transition by using it as a high-resolution velocity selector. But this is only part of the story. Using these narrow-line pulses we can make a dark velocity state where atoms are no longer excited, whose width can be controlled simply by adjusting the length of the 657 nm pulse, even to make the dark state more narrow than a photon recoil. The power of this cooling technique is that we are able to combine velocity selectivity with a velocity-dependent dark state, differentiating our scheme from traditional Doppler cooling and even previous demonstrations of narrow-line cooling. This concept, however, has been seen before in the context of Raman cooling.[22] With Raman cooling, Fourier-transform limited lineshapes have been used

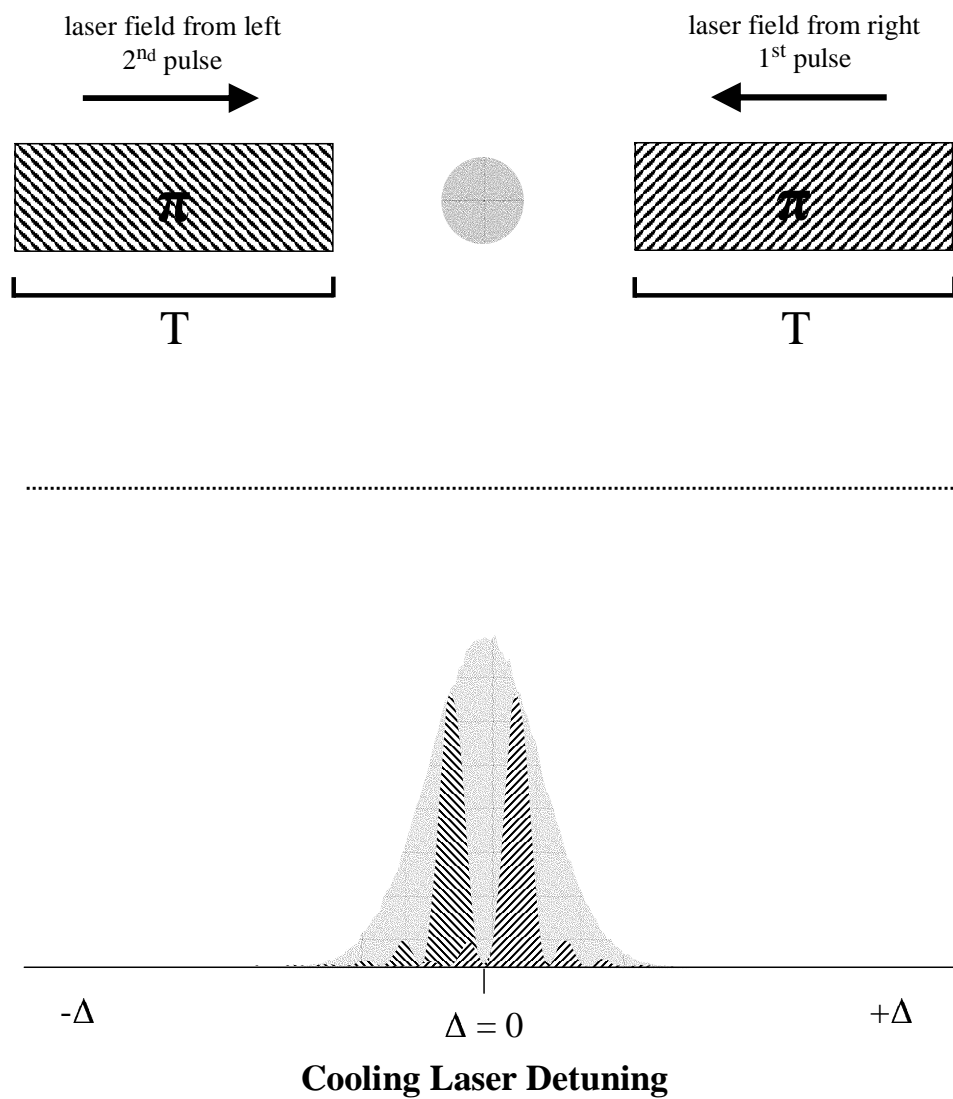


Figure 3.3: The upper figure shows how red π -pulses are incident on the atom cloud first from the right and then from the left. The lower figure shows the frequency domain picture of these pulses overlapping with two distinct velocity classes of atoms in the velocity distribution.

on two-photon transitions in Λ -systems to great effect, enabling subrecoil cooling of Cs to 3 nK in 1-D.[38]

Following the initial excitation of atoms using the narrow transition, the second part of the cooling sequence relies upon quenching the excited atomic state, which enables the fast repetition of this cooling sequence. An additional bonus of this scheme is that the quenching pulse can be engineered such that it gives the atoms an additional momentum kick in the same direction as the cooling pulse, much like in the two-photon Raman case, further speeding up the cooling process. One downside to quenching is that, although the atoms never pick up any added momentum from the spontaneous decay of 657 nm photons, the atoms will get a momentum kick in a random direction during the quenching processes due to the decay from the $^1S_0(4s5s)$ quenching level to the $^1P_1(4s4p)$ level of $1.03 \mu\text{m}$, and from the decay from the 1P_1 level to the $^1S_0(4s^2)$ ground state. Since the additional momentum is randomly directed, it averages out over time. It complicates matters, however, as these addition recoils can heat the atoms in the uncooled dimensions and can greatly affect the cooling process, especially when cooling with extremely narrow cooling pulses.

3.1.1 1-D simulations of pulsed QNLC

While the transition probability can be easily calculated, the final atomic velocity distribution due to QNLC is not so easy to obtain. As this is a random process of atom-photon interactions, a Monte Carlo (MC) approach seemed an appropriate way in which to model the QNLC process. In our simulations we seek to model how an ensemble of individual, non-interacting atoms are affected by resonant and near resonant pulsed radiation in a vacuum.

Our MC simulations use the excitation probability equation derived from the standard Rabi oscillation formula as given in equation 3.11, which details the way in which light interacts with atoms at different velocities. This equation gives the

probability of exciting an atom from the ground state to the excited state for a given laser power, laser detuning and pulse length. To calculate the final atomic velocity distribution due to cooling, we start by assigning each atom a velocity such that the initial velocity distribution of atoms is a Maxwell-Boltzmann distribution and has an rms velocity of 70 cm/s, a typical experimental value corresponding to 2.4 mK. We then use the Rabi equation (3.11) to assign the probability of the atom being excited. Rabi frequencies and pulse lengths for the simulation are chosen appropriate to the experimental 657 nm laser power in order to make π -pulses. If the atom is excited, one red recoil (1.51 cm/s) is added to its velocity in the “direction” the laser pulse is propagating. We define an axis where atoms with positive (negative) velocities are moving to the right (left). In the model, light is first incident on the ensemble of atoms from the right. The duration of this pulse will determine the width of the sinc^2 excitation function. After this, we assume that the green quenching light excites the atom, giving it an additional velocity equal to the 552 nm recoil velocity (1.79 cm/s) to the right, as well. (This initial assumption that the green light excites the atoms with 100 % efficiency is not valid under experimental conditions, due to the available laser power at that wavelength and allowable length of cooling and quenching cycle. These considerations will be taken into account in section 3.1.3.) After excitation by the 552 nm light, the atom undergoes spontaneous emission that brings it back to the ground state, gaining a velocity kick in a random direction from the recoil of an IR photon ($\lambda_{IR} = 1.03 \mu\text{m} \rightarrow v_{recIR} = 0.96 \text{ cm/s}$) and a blue photon ($\lambda_{blue} = 423 \text{ nm} \rightarrow v_{recblue} = 2.34 \text{ cm/s}$). We take the random direction of these recoils into account in the 1-D simulation by generating a random percentage of the recoil velocity and adding or subtracting that value to the velocity of the atom. We then repeat this process with cooling and quenching light incident from the left because the simulation showed that this sequence reversal was found to help maintain the symmetry of the cooling process. (This was subsequently verified in experiments, see Chapter 5.) Every atom is cycled through this

MC simulation some fixed number of times, which adds up to the total cooling time. The total experimentally allowed cooling time will be limited by the initial velocity of the atoms and the speed at which we can quench the 3P_1 state, which is directly related to the available green power. (An example of the Matlab code I used to generate these MC simulations is given in Appendix A.)

Normally when discussing narrow-line cooling, the recoil limit refers to the recoil imparted by the cooling laser. In fact this limit is deceiving in quenched cooling as we should really be considering the recoils that truly affect the final velocity of the atoms. In our specific case, photon recoils are due to the 1.03- μm and 423-nm spontaneous emissions that occur due to the quenching pulse. Our “recoil” limit is the sum (in quadrature) of these values, 2.53 cm/s. One should also note, however, that when using this pulsed-cooling method in 1-D, this recoil limit does not set a hard limit for the final achievable temperature. The limit is instead set by the width of the dark velocity state, controlled by the width of the cooling pulses, as seen in subrecoil Raman and VSCPT cooling.

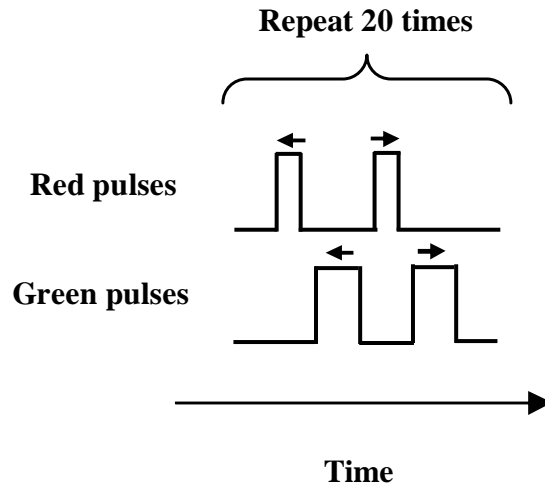


Figure 3.4: The Monte Carlo simulation uses a sequence of a red pulse from the right followed by a green pulse from the right, and then the same sequence repeated with pulses coming from the left. This cooling-quenching cycle was repeated 20 times.

To start, we simulate cooling due to red pulses, $\tau_p = 2.5 \mu\text{s}$ in duration, whose frequency is detuned $1/\tau_p$ from resonance in order to place the first zero of the sinc^2 function at zero velocity. The timing sequence goes as follows. A red pulse from the right is followed by a green pulse from the right. The green pulse transfers the excited atoms back to the ground state (assuming 100% quenching efficiency). This red-green sequence is then repeated, but with pulses incident from the left. The four-pulse cycle is repeated 20 times. A schematic representation of the sequence of cooling and quenching pulses is shown in Figure 3.4. All simulations shown in this chapter involve 100,000 atoms.

As one can easily see in Figure 3.5, detuning by $1/\tau_p$ does not lead to a single narrow velocity distribution as was expected intuitively. Even though the 20 cooling cycles would allow a resonant atom to acquire enough photon momentum kicks to reach the center of the zero-velocity dark state, as the atom approaches zero velocity it is in fact moving out of resonance with the detuned pulse and therefore becomes less and less likely to gain any additional momentum. This causes atoms to pile up into peaks at some non-zero (but near-zero) final velocity. In addition, the slope of the sinc^2 excitation probability is quite steep, causing the cooling to stop just shy of halfway between the detuning $1/\tau_p$ and zero velocity. The two central peaks do, however, fall within the dark state velocity width centered at zero velocity as expected for this detuning. Once this effect was realized, the detuning was adjusted such that the atoms would pile up at zero velocity in a single narrow peak.

A simulation repeating the pulse pattern from Figure 3.5, but changing the detuning to -207 kHz ($\sim 13.6 \text{ cm/s}$), gives a much more satisfying single cold peak, centered at zero velocity, as shown in Figure 3.6. (The broader distribution found in most of the simulation figures in this chapter shows the initial atomic velocity distribution, with a $v_{rms} = 70 \text{ cm/s}$ due to the initial blue Doppler cooling.) The second simulation (also shown in Figure 3.6) has the same timing sequence, but the length of the red pulse is $5 \mu\text{s}$, and the “cooling laser frequency” is not detuned as far from resonance, only -91

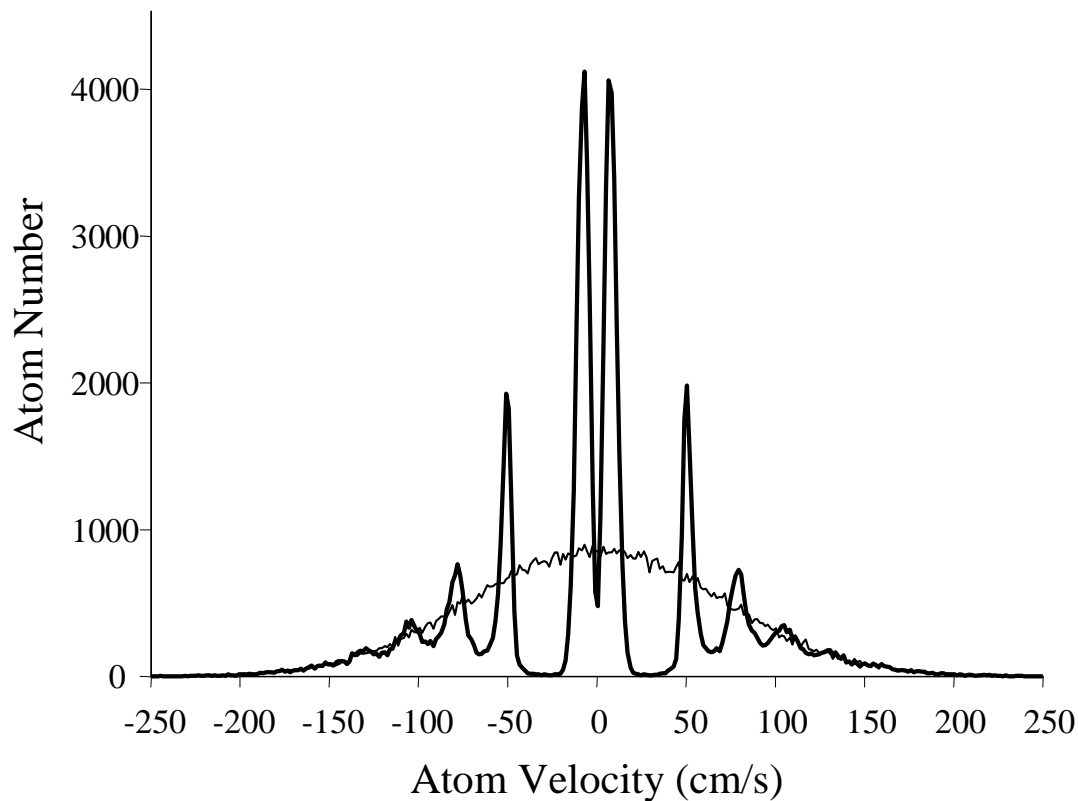


Figure 3.5: Monte Carlo simulation of QNLC with the cooling cycle consisting of a 2.5- μs red pulse followed by a 100 % efficient green pulse, both from the right, and then the same pattern repeated with pulses incident from the left. This entire cycle is repeated 20 times. Detuning at the intuitive $1/\tau_p$ to place the zero of the sinc^2 function at zero velocity does not create a distribution with a single narrow peak. The thin line shows the initial 70 cm/s atomic velocity distribution.

kHz (~ 6 cm/s), to account for the narrower excitation distribution, and, therefore, our optimum detuning is closer to zero detuning.

The simulations show that the broad initial velocity distribution has been significantly narrowed in the QNLC processes. In the simulation shown in Figure 3.6(a), the narrow peak has a full width at half maximum (FWHM) of ~ 7 cm/s, which corresponds to a v_{rms} for a Gaussian distribution of 3 cm/s, while in the simulation shown in Figure 3.6(b), the FWHM ~ 5 cm/s, corresponding to $v_{rms} = 2.1$ cm/s. Even in this idealized simulation not all of the atoms are transferred into the narrow, central peak. The 2.5- μ s pulse has a transfer efficiency of 33 %, and the transfer efficiency of the 5- μ s pulse is only about half as much, 17 %. In fact, due to the other zero excitation probability nodes of the $sinc^2$ excitation function, atoms not only get “trapped” in the zero velocity zero of the $sinc^2$, but also in the other zeros, hence the additional evenly spaced peaks in the velocity distribution. This feature has also been seen before in the experiments of Raman cooling. It turns out that there are other cooling laser pulse shapes that lead to smoother spectra when Fourier-transformed. One such pulse shape used in Raman cooling is called a Blackman pulse, which was discussed in the first Raman cooling paper.[22] A more thorough discussion of how pulse shapes affect the cooling and cold atom number is given in Reference [38]. Reichel *et al.* conclude that square pulses (like we use) are the most effective in 1-D, but for pulsed cooling in 3-D, more rounded pulses, such as Blackman pulses, transfer more atoms into a colder central peak.

The number of cooling cycles is very important to the cooling process. Shown in Figure 3.7 are simulations highlighting the difference between cooling for 20 cycles with 2.5- μ s pulses (as was the case in Figure 3.6a) and cooling for only 5 cycles. In the simulation depicted in Figure 3.6a, (dotted line in Figure 3.7), there were enough cooling photons to kick nearly all the atoms in the chosen velocity range into the central peak (or another $sinc^2$ zero), but in the new simulation (solid line in Figure 3.7) there

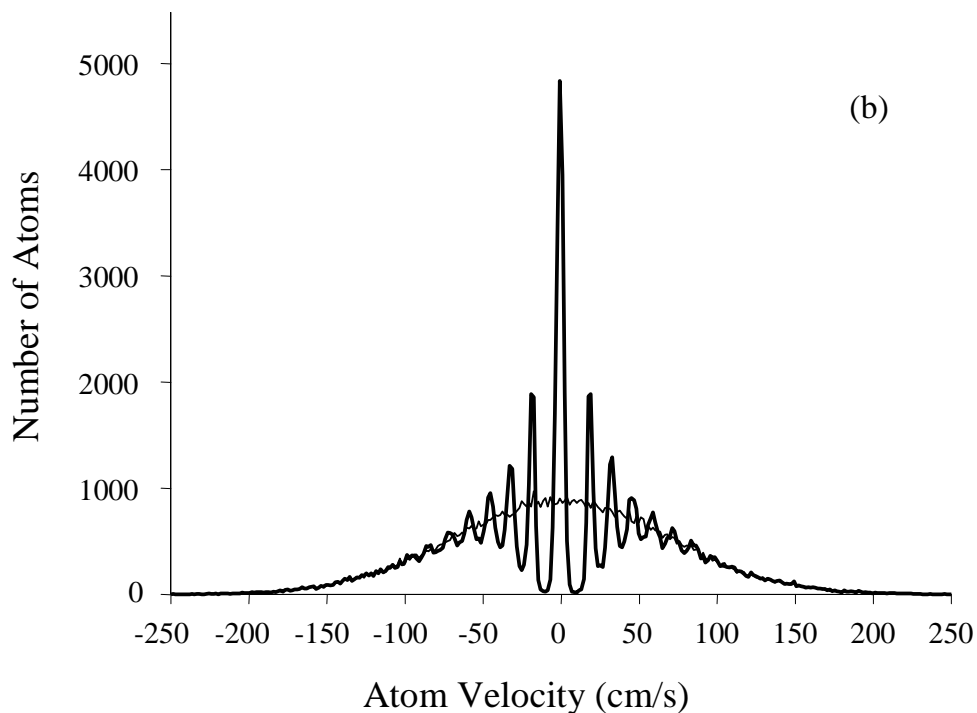
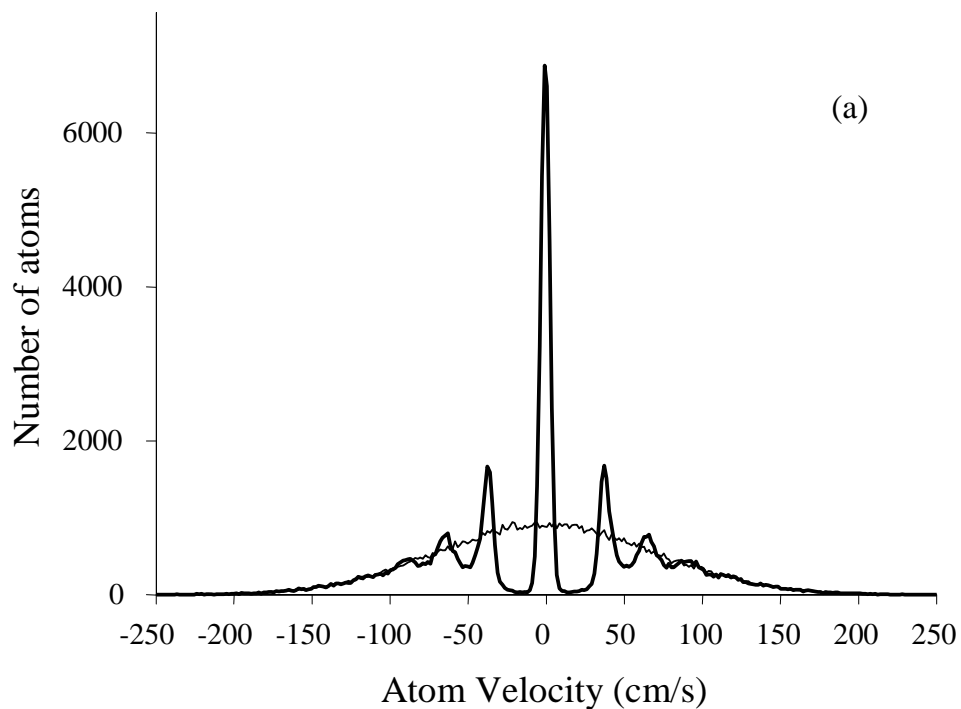


Figure 3.6: Simulated velocity distribution of the atoms after 20 cooling cycles. Each cooling cycle consisted of a cooling pulse from the right followed by a quenching pulse from the right, and then that sequence was repeated from the left. The original velocity distribution of Doppler-cooled atoms ($v_{rms} = 70$ cm/s) is shown by the thinner line in Figures (a) and (b). In distribution (a), a cooling pulse width of $2.5 \mu\text{s}$ led to a final $v_{rms} = 3$ cm/s, and in distribution (b), a cooling pulse width of $5 \mu\text{s}$ led to a $v_{rms} = 2.1$ cm/s.

have not been enough cooling cycles for the most efficient atom transfer and cooling. Due to the initial velocity (70 cm/s) of the blue-cooled atom cloud at $T = 2.4$ mK, we estimate that at most ~ 2.5 ms will be available for the entire second-stage cooling cycle, due to atoms travelling beyond the edges of the cooling beams in the uncooled dimensions.

Another notable and problematic feature becomes clear when observing the two simulations in Figure 3.6 together. One can see that more atoms can be transferred into the central peak with a shorter red cooling pulse, but with a correspondingly broader sinc^2 lineshape, which results in a broader (warmer) central velocity distribution. The velocity distribution that results from the longer 657 nm pulses is much narrower, but with fewer atoms transferred into that narrower peak. This unfortunately means that when using single frequency cooling a compromise must be made between atom transfer efficiency and atom temperature.

3.1.2 Multi-frequency pulsed QNLC

An ideal cooling scheme, of course, would transfer all the atoms into the narrowest possible distribution and not be limited to *either* a large transfer efficiency *or* the coldest atoms. Not surprisingly, this dilemma also reared its ugly head in Raman cooling experiments. There are actually a number of ways to circumvent this dilemma, all of which are only limited by the cooling time, which is in turn usually limited by the initial temperature of the cold atom cloud combined with available laser power. Many of these ideas have been explored in the context of Raman cooling.[23, 38]

It has been demonstrated with a beam of atoms that it is possible to improve atomic cooling by ramping or chirping the cooling light frequency in order to keep it in resonance with the slowing atoms [39]. In narrow-line cooling we can use this same method, as was first shown with Sr atoms [7], to excite and cool a much larger number of atoms by chirping the detuning of the cooling pulse during the cooling process. This

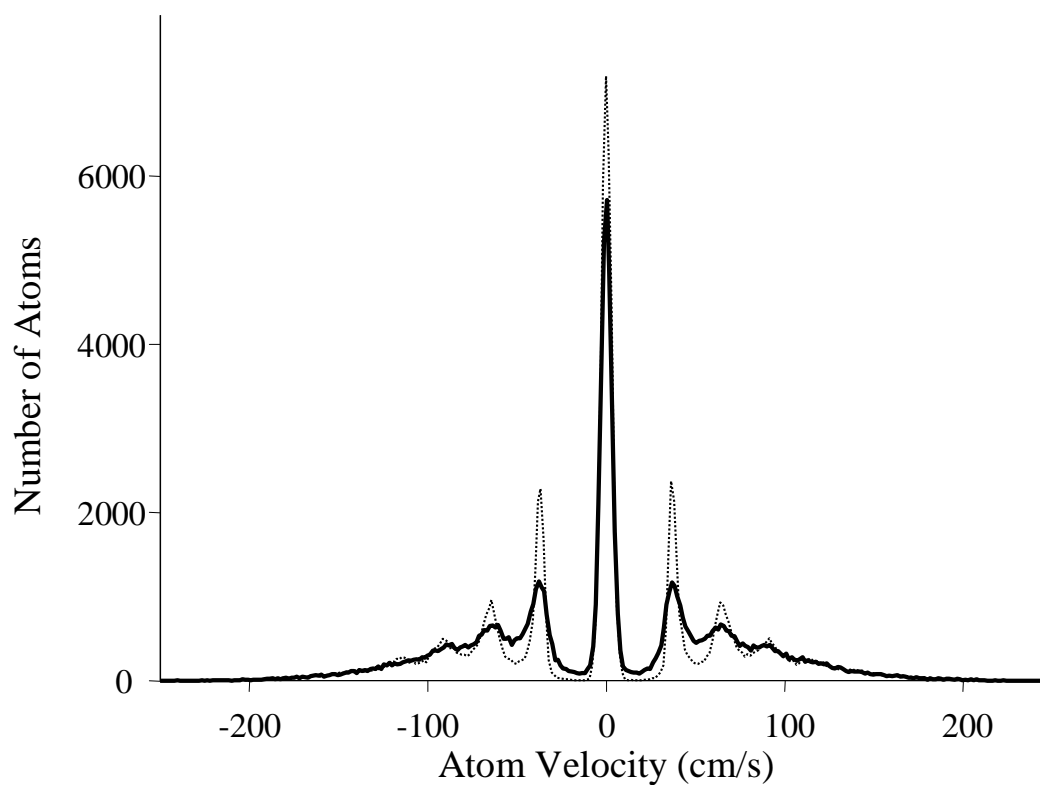


Figure 3.7: Simulated velocity distribution of the atoms after 20 cooling cycles of $2.5\text{-}\mu\text{s}$ pulses with 100 % effective quenching (dotted line) is compared to the distribution made with the same cooling processes, but stopped after only 5 cooling cycles (solid line). Approximately the same number of atoms was transferred to the central peak, but the distribution is broader.

greatly increases the number of atoms in the final velocity distribution. Of course, one has to chirp the light at a speed at which it will interact with all the atoms in any given velocity class before the light is swept out of resonance, and as the cooling time is limited by other experimental factors, this limits the frequency coverage (velocity range) of the chirp.

We wished to simulate a modified version of this idea to improve our cooling efficiency and cold atom number. Instead of a chirped pulse whose speed and duration would be limited by cooling time, we proposed to cool in multiple stages. In the first part of the cooling time, a short pulse, broad in the frequency domain, is detuned farther from resonance so as to move a large number of atoms closer to zero velocity. This is followed by a much longer pulse that is spectrally narrower in order to cool this large number of atoms into the ultracold velocity distribution. To gather up a larger percentage of atoms, more than two differently sized and detuned pulses could be used, as has also been used in Raman cooling[23]. Since the cooling pulses are relatively short π -pulses, many pulses can be cycled in the time it would have taken to chirp the frequency of the cooling beam. With spectrally broad pulses, even the atoms located in the far wings of the velocity distributions could be quickly transferred close to zero velocity for more efficient cooling.

As a demonstration of just one permutation of this multiple-pulse cooling, I have simulated cooling with two different pulse widths at three different detunings. There are 20 cycles of cooling, for easier comparison to the 20 cycles used in the previous simulations. For 7 cycles, the pulses are 2.5- μ s long, but detuned twice as far as they would be for single frequency cooling. For the next 6 cycles, the pulses remain the same length, but are set at the optimal detuning, which places the zero of the sinc^2 excitation lineshape at zero velocity. For the last 7 cycles, 5- μ s pulses are used and optimally detuned. Results of this simulation are shown in Figure 3.8.

Atoms with velocities twice as large as in the single frequency case have been

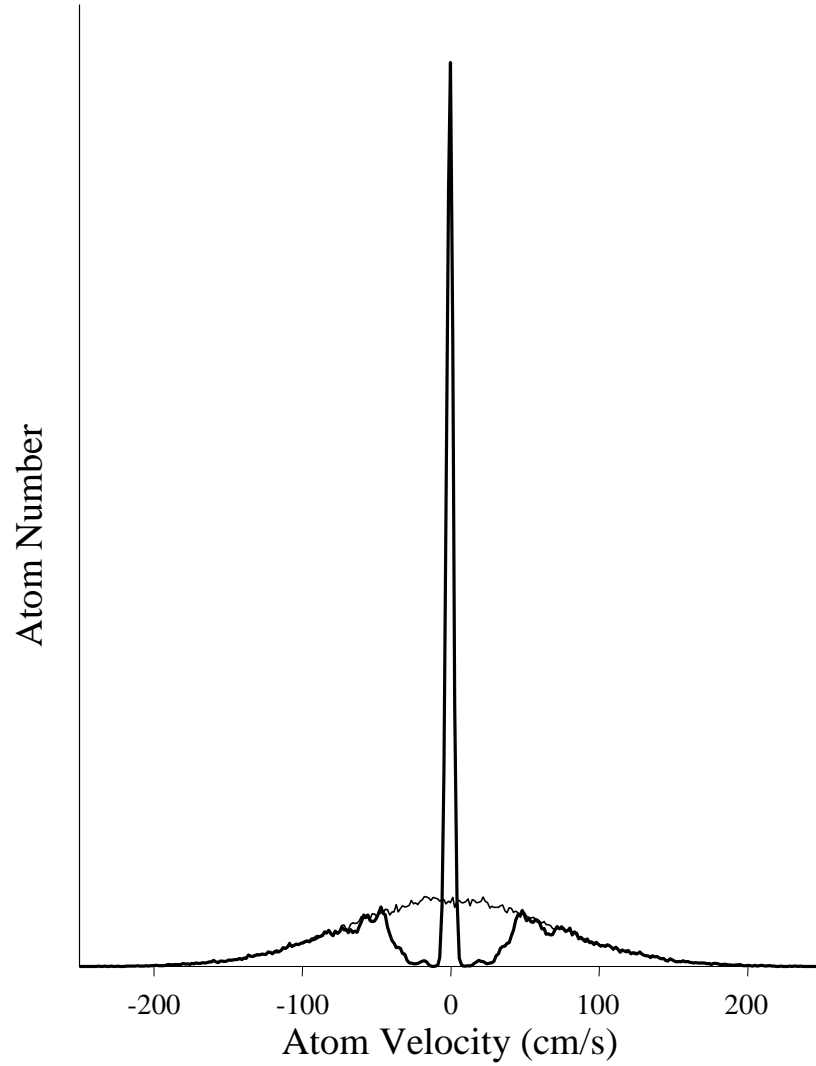


Figure 3.8: Simulated velocity distribution of the atoms after 20 cooling cycles where both the pulse duration and detuning are changed. The cooling sequence is as follows: 7 cycles of $2.5\text{-}\mu\text{s}$ pulses detuned twice as far from zero as would give the coldest distribution on its own, 6 cycles of $2.5\text{-}\mu\text{s}$ pulses at the optimal detuning for single pulse cooling, and 7 cycles of $5\text{-}\mu\text{s}$ pulses at optimal detuning. Each cooling cycle consisted of a cooling pulse from the right followed by a quenching pulse from the right, and then that sequence repeated from the left. The FWHM of this distribution is 5 cm/s , corresponding to $v_{rms} = 2.1\text{ cm/s}$, $T = 2.1\text{ }\mu\text{K}$. The original velocity distribution of Doppler-cooled atoms is depicted by the thin line. The transfer efficiency from this original distribution to the narrow peak is 42% .

transferred in towards zero velocity with the first and second sets of pulses, and the third set of pulses narrows the velocity distribution. Atoms that had previously been caught in the other zeros of the sinc^2 excitation probability have now been transferred into the narrow, ultracold central peak, with the same v_{rms} as was given by the 5- μs pulse by itself in the previous simulation, 2.1 cm/s, but now with a transfer efficiency of 42 % rather than 17 %. Given a sufficient cooling time, pulses could be detuned farther and then slowly walked in to the optimal detuning for the greatest transfer efficiency. There are many other variations on this approach using different pulse widths and detunings, but ultimately the cooling time limitations of the actual experiment will dictate how to best use this multi-pulse, variable detuning method.

3.1.3 Simulating experimental conditions

In our first experimental attempt at 1-D quenched cooling, we knew our green power would be limited to about 20 mW, so we wanted to include this in our simulations. In order to approach 100 % transfer from the excited state back to the ground state, we would have to use a green pulse of long duration. Unfortunately, rapid cooling is important so that the warmer atoms will not move out of the trapping region during this cooling time due to the finite width of the trapping beams, and we must compromise between cooling time and cooling efficiency. If the green pulses could be half as long in duration, we could essentially perform twice as many cooling cycles. To increase the quenching rate we can retroreflect the green light for the quenching pulses instead of having the quenching light come into the trap in the same direction as the red pulses. This would speed up the cooling since it effectively doubles the amount of green light incident on the atoms, but it reduces (by about the same factor) the cooling effect by not using the green photon recoil to assist in the actual cooling. Under experimental conditions we would be using linearly polarized light to excite these transitions in one dimension, as the photon will always be absorbed to excite the atom from the

$^1S_0(m = 0)$ to the $^3P_1(m = 0)$ state in our MOT geometry. And retroreflecting the green also effectively doubles the cooling rate since we can apply two (short) red cooling pulses before needing a (long) quenching pulse. It is also much easier to implement experimentally as we are retroreflecting the quenching light rather than needing additional green beams, which would also reduce the available power. Unfortunately, now that we are no longer using the recoil of the green light to our advantage during cooling, we must take the direction of its random recoil into consideration. This increases the “recoil limit” of the cooling process by including the green ($v_{rec} = 1.73$ cm/s) as well as IR and blue recoil photons, giving a recoil limit of ~ 3 cm/s, rather than 2.5 cm/s. Figure 3.9 compares this new case of retroreflected green quenching (solid line) to previous sequential quenching (dotted line). The cooling is not quite as efficient as in the ideal case, as the 552 nm recoils are no longer helping to speed the cooling, and are now even heating the atoms half of the time.

With less than 100 % transfer efficiency for the quenching transition, not all the atoms will return via the quenching transition to the ground state during the cooling process, leaving some cold atoms undetectable in the excited state, and reducing the effectiveness of the cooling. This also means that at the end of the cooling cycles, some atoms will still be excited, reducing the number of atoms contributing to the final velocity distribution. In practice one could wait for these atoms to decay naturally, which would extend the cooling time by ~ 400 μ s, the lifetime of the narrow transition. Alternatively, we could employ a long green pulse after the cooling and quenching cycles guaranteeing that nearly all of the atoms would be transferred back to the ground state for detection and use in the experiment. This end of cycle green pulse is included in all the following simulations.

After 20 cooling cycles we can compare the results of simulations with different quenching efficiencies. Figures 3.10(a) and 3.10(b) show 70 % and 30 % quenching efficiency, respectively (solid lines), compared to 100 % quenching efficiency (dotted

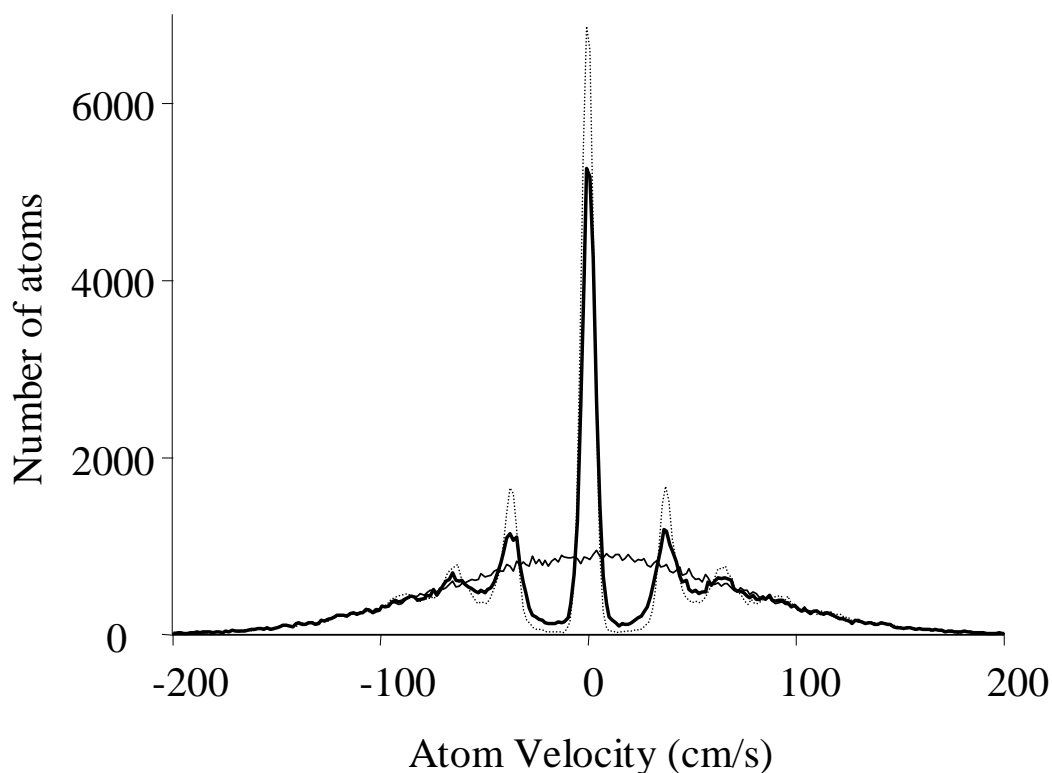


Figure 3.9: Simulated velocity distribution of the atoms after 10 cooling cycles, with red cooling pulses of $2.5\text{-}\mu\text{s}$ duration. Each cooling cycle consisted of a cooling pulse from the right followed by a cooling pulse from the left, and then a pulse of quenching light from both directions simultaneously transferred some fraction of the excited population back to the ground state. To help preserve symmetry, the process was repeated, starting with a pulse from the left. In the figure the solid line shows the final velocity distribution if the quenching light is 100 % efficient but only simulated to quench in a “retroreflected” beam configuration. This should be compared to the dashed line, which shows the velocity distribution from Figure 3.6(a) where the quenching photons come from the same direction as the preceding red pulse and, hence, directly assist in the cooling.

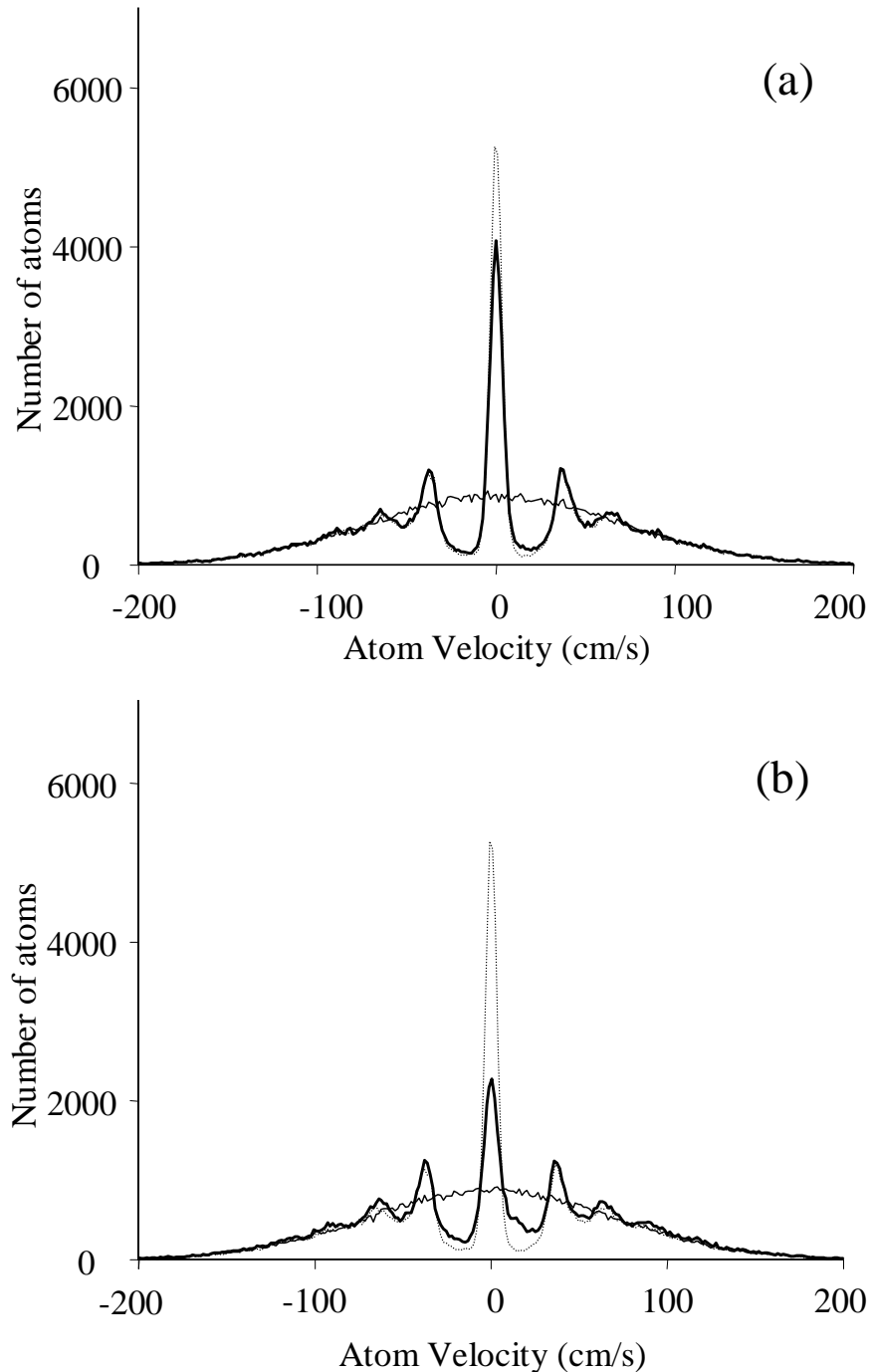


Figure 3.10: Simulated velocity distribution of the atoms after 10 cooling cycles, with red cooling pulses of $2.5\text{-}\mu\text{s}$ duration. Each cooling cycle consisted of a cooling pulse from the right followed by a cooling pulse from the left, and a pulse of quenching light from both directions simultaneously to transfer some fraction of the remaining excited population back to the ground state. To help preserve symmetry, the process was repeated, starting with a pulse from the left. Distributions (a) and (b) (solid lines) used quenching pulses with only 70 % and 30 % efficiency, respectively, in transferring the atoms back to the ground state. For comparison, the dotted line distributions in (b) and (c) show 100% efficient quenching with a single “retroreflected” quenching pulse after the pair of sequential red cooling pulses.

lines, solid line in Figure 3.9). With reduced quenching efficiency, the simulations show a warmer distribution and the holes in the velocity distribution are not dug out as deeply, causing fewer atoms to be transferred to the central narrow peak. In simulations with imperfect quenching efficiency, asymmetry in velocity distributions becomes apparent. This is due to the fact that if an atom is not quenched it has a high probability of being heated by a subsequent pulse from the opposite direction. In this simulation I have found that I can minimize the asymmetry by alternating the starting direction after every two pulses, as was found for the 100 % green efficiency case. This greatly reduces the asymmetry, but does not eliminate it, as can be seen most clearly in the 30 % efficient quenching simulation, Figure 3.10(b). From these simulations it is abundantly clear that the amount of green power at our disposal will greatly affect our experimental cooling results.

3.2 3-D QNLC using simultaneous cooling and quenching

We would like to extend this QNLC scheme to cool atoms in three dimensions. The main reason for this is that our ability to create ultracold atomic distributions in one dimension does not help retain the atoms for long times. The velocity of the atoms in the remaining two dimensions has not been reduced by the 1-D cooling and the atoms escape in directions transverse to the cooling beams. Also, 1-D cooling does not help to reduce the velocity dependent frequency shifts of the Ca frequency standard. It is actually the velocity of the atoms *transverse* to the 1-D optical clock spectroscopic beams that creates one of the frequency shifts we are trying to eliminate with this second-stage cooling, so we would have to cool in at least two dimensions to achieve that goal. Moreover, most other applications would benefit from the increased phase-space density associated with 3-D cooling.

The step-wise excitation approach we used for 1-D cooling can be extended to three dimensions, as was shown in Raman cooling [23]. For its application to the calcium

system, we carefully consider the pulse sequence required for 3-D cooling. Difficulties arise in trying to deal with the continuous expansion of the atom cloud in the directions that have not yet been cooled. Taking into consideration the reduction of the velocity distribution during the cooling time and the difficulty of providing pulsed red cooling beams in all three dimensions at the same time, a good approach would be to alternate cooling pulse directions, beginning with cooling in two dimensions for 0.5 ms, and then in the other dimension for 1 ms. Implementing such a cooling sequence would add significant complication to the experimental setup, but would be possible.

When trying to both cool *and* trap the atoms it becomes experimentally advantageous to implement the continuous cooling and quenching approach demonstrated first by Binnewies *et al.* at the Physikalisch Technische Bundesanstalt (PTB).[40] They used a scheme where the cooling and quenching light were simultaneously incident on the atoms, rather than applied sequentially. The major difference between our 3-D approach when compared to that used at PTB is the quenching transition utilized. There are some significant differences between our choice of the green $^3P_1 \rightarrow ^1S_0(4s5s)$ transition at 552 nm and PTB's choice of the blue $^3P_1 \rightarrow ^1D_2(4s4d)$ transition at 453 nm, chosen primarily by the availability of lasers in both groups. These two transitions have similar Einstein A coefficients, with the linewidth (Γ) of the 1D_2 state equal to $1.4 \times 10^7 \text{ s}^{-1}$ [40] and for the 1S_0 state, $\Gamma = 3.3 \times 10^7 \text{ s}^{-1}$ [41]. The factor of 2 slower spontaneous decay from the 1D_2 state to the 1P_1 state actually accelerates the pumping processes, since the pumping rate is proportional to $1/\Gamma$, where Γ is the decay rate of the upper state in the three level system. This results in more effective cooling for the same relative power. This advantage gained by using 453 nm pumping is offset by the fact that when using dye lasers to excite these transitions the dyes used for green lasers are generally more powerful and longer-lived than those for the blue.

The lack of sublevel structure in the two 1S_0 states severely restricts the allowed transition paths when using 657 nm cooling and 552 nm quenching light. The selection

rules only allow transitions from the ground 1S_0 state through the 3P_1 m-levels to the upper 1S_0 state with linearly polarized light with both fields parallel (allowed $m=0 \rightarrow m=0 \rightarrow m=0$), or transitions using circularly polarized laser light that must differ in direction (σ^+ or σ^-) between the red and green transitions (Clebsch-Gordan coefficients are all 1 for these transitions). The 453 nm $^3P_1 \rightarrow ^1D_2$ transition has favorable, but not ideal Clebsch-Gordan coefficients (6:1), where more photons will be absorbed for transitions where the green and red light have the same circular polarization, but the atoms will absorb some quenching photons of the opposite polarization, heating the atomic sample.

With the cooling and quenching beams turned on simultaneously throughout the cooling process, the atoms can be continuously cycled and cooled in a manner similar to Doppler cooling on just two atomic levels (albeit with a larger incurred recoil velocity due to the added quenching and spontaneous emission photons). In fact, the three-level QNLC system can be reduced to an equivalent two-level system with an effective transition linewidth equal to the quenching rate plus the linewidth of narrow transition (virtually negligible in the case of Ca) as discussed by Sterr *et al.* in Reference [42].

We can write the Hamiltonian for this system as $H = H_0 + H_{lightfield}$, where H_0 is the internal atomic energy and $H_{lightfield}$ is the same as given in equation 3.6, but written for our three-level system as

$$H_{lightfield} = -e\vec{E}_{01} \cdot \vec{d}_{01} - e\vec{E}_{12} \cdot \vec{d}_{12} \quad (3.12)$$

The Rabi frequency Ω is defined as in equation 3.9, and can be related to the saturation intensity I_S , defined such that

$$\Omega_{ij}^2 = \frac{I_{0,ij}}{2I_{S,ij}} \Gamma_{ij}^2 \quad (3.13)$$

with

$$I_S = \frac{hc\pi\Gamma_{ij}}{3\lambda_{ij}^3} \quad (3.14)$$

where i and j designate the energy levels of the transition, Γ_{ij} is the decay rate between levels i and j , $I_{0,ij}$ is the intensity of the laser light exciting the transition ($I_0 = E_0^2$ from equation 3.7), and λ_{ij} is the wavelength of the transition $i \rightarrow j$. (The expressions for I_S and Ω are derived in Appendix B.)

A set of coupled, time-dependent equations can be formed from this Hamiltonian acting on the atomic wavefunction, as was done for solving the two-level problem of equations 3.1 through 3.10. The three-level case gives a set of 9 coupled equations of motion instead of just two. In reference [43], Whitley and Stroud obtain these 9 coupled equations of motion, which completely describe the three-level system. Taking into consideration that, for our system, the decay rate from the upper level is much faster than from the intercombination line, a simpler set of solutions can be derived if the quenching laser is only minimally detuned. Not only can we neglect two-photon transitions in this case, but it allows us to adiabatically eliminate the upper state, leaving an effective two-level system with an effective decay rate, Γ_{eff} , which can be written as

$$\Gamma_{eff} = \Gamma_1 + r_{12} \quad (3.15)$$

where r_{12} was the pumping rate from state $|1\rangle$ to state $|2\rangle$,

$$r_{12} = \frac{\Gamma_2 \Omega_{12}^2}{4\delta_{12}^2 + \Gamma_2^2} \quad (3.16)$$

and where δ_{12} is the detuning of the quenching laser from resonance. The Rabi frequency of the $|1\rangle \rightarrow |2\rangle$ transition (Ω_{12}) and the decay rate Γ_2 are defined in the energy-level diagram given in Figure 3.11, which shows the relation between the original three-level system and the reduced two-level system.

The dependence of r_{12} on the Rabi frequency, as given in equation 3.16, actually gives quenched cooling the additional (and powerful) ability to tune the linewidth of the effective Doppler cooling transition simply by changing the quenching power, as first pointed out by Wallis and Ertmer.[35] With this in mind, one can envision a cooling

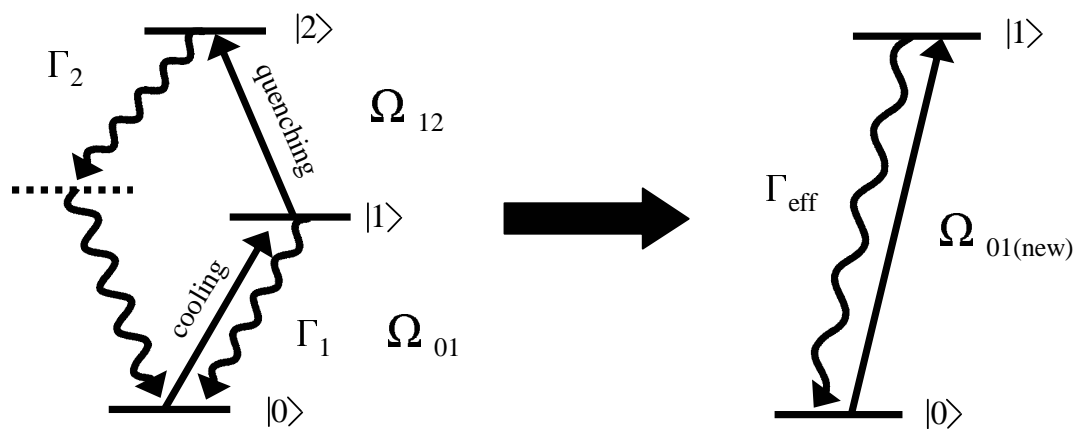


Figure 3.11: In our case of quenched cooling with ^{40}Ca , the three-level quenched cooling system can be reduced to a two-level system with a single effective lifetime, Γ_{eff} .

procedure that starts with the use of high-power quenching light to create a broad transition linewidth (i.e., with its wide Doppler coverage and fast cooling rate) to cool a large range of velocities and then concludes with reduced quenching power for narrow-line cooling and its associate colder temperatures. Unfortunately, with the quenching power presently available to us, we are unable to increase the linewidth enough to cover the entire Doppler-broadened distribution and we must instead broaden the red cooling light in order to extend the capture range of the second-stage cooling transition.

Binnewies *et al.* have described the theory behind and implementation of their 3-D cooling scheme in Reference [40]. They started with first-stage cooling and trapping of ^{40}Ca atoms performed using the standard broad 423 nm transition. Then they overlapped the blue MOT with a two-color 657 nm and 453 nm MOT, whose red beams had the same laser beam polarizations as the beams for the blue trap. This red laser light was spectrally broadened using harmonic frequency modulation at 15 kHz, with a modulation width of 1.4 MHz, while the center of the frequency was tuned $2\pi \times 280$ kHz below resonance to induce cooling. This created a comb of frequencies with comb teeth spaced 15 kHz apart. The spacing of these comb teeth is important in the sense that a large number of comb teeth spaced closely will spread the power too thinly, reducing atom excitation, but if the teeth are spaced farther apart to increase the power in each comb tooth, then atoms may fall into velocity holes, becoming no longer resonant with the trapping light. This method was modelled after Katori's use of modulated light to increase the Doppler coverage [33] and broadband cooling used previously with atomic beams by Zhu *et al.*[44].

Two different cooling regimes are discussed in the PTB paper, both assuming the absence of a magnetic field gradient. The first is the narrow-line Doppler cooling regime, where atoms feel a constant damping force by the comb of light. Eventually the atoms slow to the point at which they are out of resonance with the cooling laser. However, there is still a non-zero probability of excitation, unlike in our step-wise pulsed cooling

scheme. Binnewies *et al.* refer to this as a “grey-state” to differentiate it from the dark state of Raman, VSCPT, and pulsed narrow-line cooling. The final velocity distribution cannot be as narrow as in a pulsed-cooling scheme, but can in principle be as low as a fraction of a recoil. However, one must wait for the atoms to fall into the grey-state, extending the cooling time much in the same way as was needed in VSCPT, where the atoms were also not actively pumped into the dark state, but had to fall there due to Brownian motion of the atoms. When the necessary and significantly smaller magnetic field gradient is turned on for trapping, the atoms will feel a force towards the center of the trap, pushing them out of the “grey state” and raising the final temperature of the atom cloud, giving a limit for trapped atom temperatures of a few recoils.

The recoils gained through the quenching process begin to affect the 3-D cooling results, as a random recoil from cooling in one direction heats the other directions. This may set a real limit for the final cold atom temperature to about the quenched recoil limit of $T = 4 \mu\text{K}$ (in our case due to green, IR and blue recoils added in quadrature). For the PTB experiments these recoils were the limiting factor in the final trapped atoms temperatures of $6 \mu\text{K}$ (or 3.4 cm/s , nearly the calculated effective recoil velocity for their system.) There may be a clever way to eliminate these large recoils and reduce the limit back to a single red recoil. Recall that the reason we are using a quenched-cooling scheme is that our initial atom cloud is too warm to be cooled directly with the narrow transition. After quenched cooling, we could have 3-D temperatures of a couple microkelvin. At the end of the cooling sequence, when the atom cloud has reached this temperature, we could turn off the quenching beams and simply use the red transition itself for extra cooling. We would have the luxury of waiting for the atoms to decay from the excited state, as the atoms are only moving at a couple of centimeters per second and the decay time of the transition is $\sim 400 \mu\text{s}$, allowing a number of red-only cooling cycles to occur before atoms would begin moving out of the cooling region. This additional narrow-line cooling would bring our 3-D limit to 1.51 cm/s or $\sim 1 \mu\text{K}$.

3.3 Third-stage 1-D QNLC

In my previous discussion of 1- and 3-D cooling methods based on QNLC, the final temperatures attained from the cooling would be limited by the available cooling time, which in turn is limited by the warm initial temperature of the atom cloud and available quenching laser power. However, after the 3-D cooling is complete, we can expect atomic temperatures approaching $4 \mu\text{K}$. With distributions this narrow, the allowed cooling time becomes much longer, as the atoms are only moving at an average velocity of less than 3 cm/s , rather than 70 cm/s as achieved with single-stage 423 nm blue cooling alone. Our original 1-D QNLC methods can now be used to further cool the already cold atoms to far below the recoil limit.

Simulations of third-stage QNLC are initiated with atoms having an rms velocity of 4.5 cm/s , which corresponds to a temperature of $10 \mu\text{K}$, a typical result for second-stage cooling. In the two simulations in Figure 3.12, plot (a) depicts single frequency 1-D third-stage cooling with a cooling pulse (τ_p) $15 \mu\text{s}$ in duration. The optimal detuning in this cold initial velocity regime is actually slightly more than the inverse of the pulse width. Now that the atoms are initially so cold, a couple of photon recoils can easily push atoms into the first-order *sinc*² dark resonance. Unfortunately, it is much easier for an atom to acquire too many recoils and overshoot the first-order zero, landing instead in a higher order *sinc*² zero. I believe that the slightly larger than expected detuning helps to increase the probability that the atoms will end up near zero velocity. This simulation uses eight cycles, with each cycle consisting of a cooling pulse from the right, a cooling pulse from the left, and a quenching pulse, followed by a similar pulse sequence, but with pulses coming first from the left. The sequence reversal becomes even more important using narrower pulses in third-stage cooling. The narrow central peak in Figure 3.12(a) has a FWHM $\sim 1.2 \text{ cm/s}$, corresponding to a mean kinetic energy of 700 nK . Plot (b) uses multiple pulses with 5 cycles of $15\text{-}\mu\text{s}$ pulses and 8 cycles of

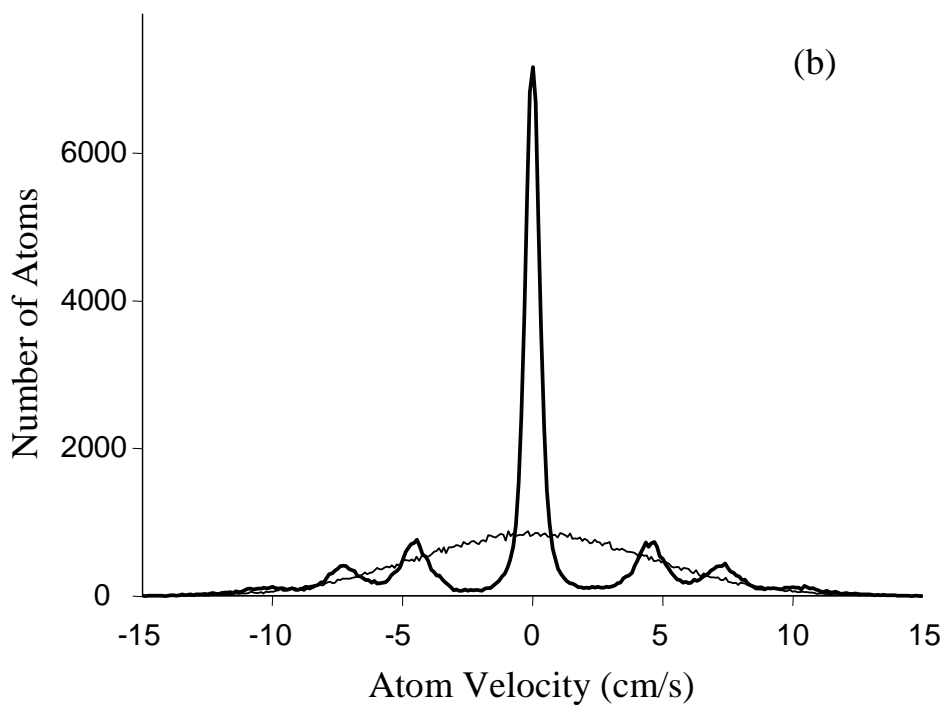
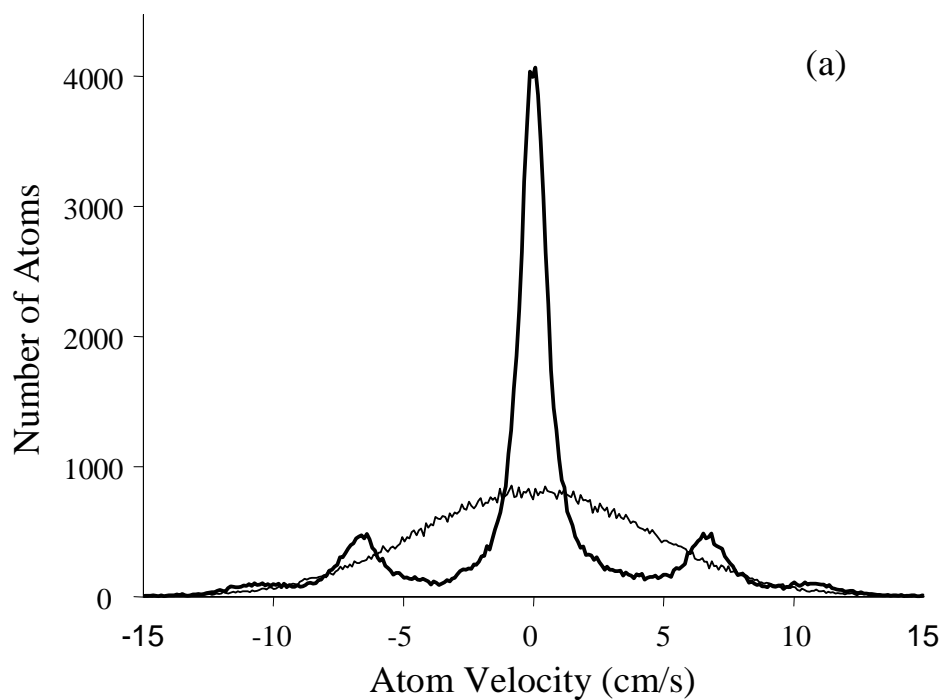


Figure 3.12: Simulated velocity distribution of the atoms after third-stage QNLC. Plot (a) was created with 8 cycles (right-left-quench-left-right-quench) of quenched pulsed cooling, where the cooling pulses were 15 μ s in duration. In plot (b), 5 cycles of 15- μ s cooling pulses and then 8 cycles of 25- μ s pulses were used. The broader distributions (thin line) show the initial second-stage-cooled velocity distribution at 4.5 cm/s.

25- μ s pulses, resulting in a FWHM ~ 0.64 cm/s, which corresponds to a mean kinetic energy of 200 nK. By starting with a much narrower initial atomic velocity distribution and using long (> 15 μ s) pulses with their narrower velocity selectivity, we should be able to cool well into the subrecoil regime, with resultant temperatures of just a few hundred nanokelvin.

One thing we have learned from these third-stage simulations is that the majority of cooling occurs in just the first cooling cycle. With small numbers of pulses needed for this additional cooling in 1-D, very little transverse heating would occur in the other two dimensions, opening the door to possible subrecoil cooling in three dimensions. The achievable 1-D temperatures would be limited by our ability to create longer and longer pulses to interact with narrower and narrower velocity classes of atoms, limited eventually by the natural lifetime of the transition.

Another way in which we could perform extra cooling of our ultracold 3-D distribution would be to use simultaneous cooling and quenching in one dimension. This would be different from the pulsed cooling in the sense that we could use the adjustability of the green power to affect the cooling transition linewidth, rather than changing pulse lengths and detuning. By slowly reducing the quenching power to zero, the cooling limit in 1-D would be half a recoil according to Doppler theory for cooling on a narrow line, which corresponds in Ca to a temperature of 273 nK.

Of course, if we are using a continuous cooling scheme we still have to worry about Doppler coverage, even when starting with microkelvin atoms, as the Doppler width of the cold atoms is about 60 kHz and the width of the red transition is only 400 Hz. The addition of simultaneous quenching light does broaden the line considerably, but with the powers we use, we can only broaden the line to < 10 kHz. In order to produce the narrowest final velocity distributions it would still be better to use the pulsed method with the control over pulse shaping that it enables. (Note: Sr atoms benefited from additional single-frequency, 3-D cooling performed after the initial 3-D

broadened-spectrum cooling and trapping.[45] However, this process nearly doubled the cooling cycle length, and Sr has the advantage of a photon recoil two times larger than that of Ca, making it difficult to apply such a method to our Ca system.)

3.4 Summary of simulation results

These simulations have been very instructive in the subtleties of 1-D QNLC. We have shown that in using single-frequency cooling there will be a compromise between using short cooling pulses and achieving high transfer efficiencies, and using longer pulses and achieving lower transfer efficiencies, but colder atomic temperatures. There are many multiple-pulse schemes that can be employed to eliminate the need for this compromise, but their practicality is limited if one cannot supply enough quenching power to speed up the cooling process. Asymmetries will occur in the final velocity distribution due to the fact that our method of pulsed cooling begins in one direction, but by alternating the direction of the first pulse of a pair of pulses we can remove most of the asymmetry except in cases with minimal green quenching efficiency. (With twice as much available 657 nm cooling power we could avoid this problem completely by pulsing on the two antiparallel cooling beams simultaneously, followed by a standing-wave quenching pulse.) We now know that the final atom temperatures are quite sensitive to the detuning of the red cooling laser and as the excitation probability spectrum becomes narrower, the sensitivity becomes greater. Cooling laser drift rates will greatly affect the experimental QNLC results. We also have learned that the optimal detuning for the coldest distributions is less than $1/\tau_p$ for 2.5- and 5- μ s pulses, and greater than $1/\tau_p$ when cooling with pulses with $\tau_p > 15 \mu$ s. We have discovered that the number of cooling-quenching cycles is critical to the final velocity distribution temperature and transfer efficiency when starting with millikelvin temperature atoms. The amount of available green quenching power will be a big factor in the efficiency of our cooling, so it will be advantageous to shorten the quenching pulse and use more cooling cycles

in the same amount of available total cooling time. This is not so much the case for cooling atomic distributions with initially microkelvin temperatures and using pulses $< 15 \mu\text{s}$, as most of the cooling then occurs in the first cooling cycle. However, as we use longer and longer pulses and more complicated pulse sequences, the amount of quenching power will again begin to affect the quality of the cooling. These simulations have explored the most relevant parameter space of 1-D QNLC and will help guide us in our experimental exploration of this novel cooling scheme in ^{40}Ca .